

Northumbria Research Link

Citation: Zhang, Luqi, Yuan, Jinhui, Cheng, Yujun, Mei, Chao, Zhou, Xian, Wu, Qiang, Yan, Binbin, Wang, Kuiru, Yu, Chongxiu and Sang, Xinzhu (2022) Supercontinuum and frequency comb generations in the slot SiC waveguide with four zero-dispersion wavelengths. *Optik*, 266. p. 169561. ISSN 0030-4026

Published by: Elsevier

URL: <https://doi.org/10.1016/j.ijleo.2022.169561>
<<https://doi.org/10.1016/j.ijleo.2022.169561>>

This version was downloaded from Northumbria Research Link:
<https://nrl.northumbria.ac.uk/id/eprint/49609/>

Northumbria University has developed Northumbria Research Link (NRL) to enable users to access the University's research output. Copyright © and moral rights for items on NRL are retained by the individual author(s) and/or other copyright owners. Single copies of full items can be reproduced, displayed or performed, and given to third parties in any format or medium for personal research or study, educational, or not-for-profit purposes without prior permission or charge, provided the authors, title and full bibliographic details are given, as well as a hyperlink and/or URL to the original metadata page. The content must not be changed in any way. Full items must not be sold commercially in any format or medium without formal permission of the copyright holder. The full policy is available online: <http://nrl.northumbria.ac.uk/policies.html>

This document may differ from the final, published version of the research and has been made available online in accordance with publisher policies. To read and/or cite from the published version of the research, please visit the publisher's website (a subscription may be required.)

Supercontinuum and frequency comb generations in the slot SiC waveguide with four zero-dispersion wavelengths

Luqi Zhang^a, Jinhui Yuan^{a,b,*}, Yujun Cheng^a, Chao Mei^b, Xian Zhou^b, Qiang Wu^{c,d}, Binbin Yan^a, Kuiru Wang^{a,*}, Chongxiu Yu^a, Xinzhu Sang^a

^aState Key Laboratory of Information Photonics and Optical Communications, Beijing University of Posts and Telecommunications, Beijing 100876, China

^bResearch Center for Convergence Networks and Ubiquitous Services, University of Science & Technology Beijing (USTB), Beijing 100083, China

^cDepartment of Physics and Electrical Engineering, Northumbria University, Newcastle upon Tyne, NE1 8ST, United Kingdom

^dKey Laboratory of Nondestructive Test (Ministry of Education), Nanchang Hangkong University, Nanchang 330063, China

**Corresponding authors. E-mail: yuanjinhui81@bupt.edu.cn (J. Yuan), krwang@bupt.edu.cn (K. Wang).*

Abstract: In this paper, a slot SiC waveguide with four zero-dispersion wavelengths (ZDWs) is proposed for the supercontinuum (SC) and frequency comb generations. The four ZDWs are located at 1089, 1656, 2222, and 3113 nm, respectively. The effects of the pump wavelength, peak power, pulse width, and waveguide length on the SC generation are discussed when the waveguide is pumped near the first ZDW and the third ZDW in the anomalous dispersion region, respectively. While pumping at 1300 and 2450 nm, a near-infrared SC covering from 873 to 2444 nm and a mid-infrared SC extending from 1349 to 4727 nm with good coherences are obtained, respectively. By utilizing a 50-pulses pump source at a repetition rate of 1 GHz, we also investigate the SC-based frequency comb generation.

Keywords: Slot SiC waveguide, Supercontinuum generation, Frequency comb generation

1. Introduction

The supercontinuum (SC) sources greatly promote the developments of optical communication, precision frequency metrology, molecular detection, and biomedical science [1-4]. At present, the commonly used nonlinear materials for the SC generation mainly include Group IV materials (Si, Ge, SiGe, and Si₃N₄), chalcogenide glasses (As₂S₃, As₂Se₃, and GeSbS), and Group III-V compounds (AlN, AlGaAs, and InGaP) [5-7]. Until now, some researchers have reported the SC generations in the waveguides based on these materials [8-17].

The suitability of other nonlinear semiconductor materials for the SC generation is still being explored. The SiC could be a potential candidate for the nonlinear integrated optics due to its relatively high refractive index (2.6 at 1.55 μm [18]), relatively strong Kerr nonlinear index (on the order of 10^{-18} m^2/W [19]), and wide bandgap (2.4-3.2 eV [20]). Among the main polytypes of crystalline structures for the SiC, 4H-SiC possesses a wider bandgap (3.2 eV), which contributes to the large transparency window (0.37-5.6 μm [21]). In recent years, there have been some investigations on the nonlinear optics by utilizing the SiC material. Zheng et al. demonstrated four-wave mixing (FWM) process in the 4H-SiC microring resonator [22]. Xing et al. proposed the amorphous SiC ring resonator for efficient wavelength conversion through the FWM effect [23]. Xu et al. achieved the third-order parametric conversion in a Ge-SiC-Ge hybrid waveguide [24]. Wang et al. utilized the 4H-SiC

microresonators to investigate a series of nonlinear processes, including frequency conversion, cascaded Raman lasing, and Kerr frequency comb [20]. Zheng et al. preliminarily achieved the SC generation with a 300-nm bandwidth in the 4H-SiC waveguide [25].

In this paper, we design a slot SiC waveguide, whose four zero-dispersion wavelengths (ZDWs) are located at 1089, 1656, 2222, and 3113 nm, respectively. The effects of the pump pulse and waveguide parameters on the spectral width, first-order coherence, and flatness of the generated SC are investigated. When the pump pulse with wavelength of 1300 nm, peak power of 200 W, and width of 100 fs is launched into the 5.4-mm-long slot SiC waveguide, the generated near-infrared SC spans from 873 to 2444 nm, covering 1.49 octaves. When the pump pulse with wavelength of 2450 nm, peak power of 2.6 kW, and width of 100 fs is launched into the 2.2-mm-long slot SiC waveguide, the generated mid-infrared SC extends from 1349 to 4727 nm, covering 1.81 octaves. Finally, the SC-based frequency combs are obtained while using a 50-pulses pump source at a repetition rate of 1 GHz.

2. Theoretical model

In order to understand the SC generation dynamics, the numerical simulations have been done by the modified generalized nonlinear Schrödinger equation (GNLSE) [26]

$$\frac{\partial}{\partial z} A(z, T) + \frac{\alpha}{2} A(z, T) - \sum_{m \geq 2} \frac{i^{m+1}}{m!} \beta^{(m)} \frac{\partial^m A(z, T)}{\partial T^m} = i\gamma \left(|A|^2 A + \frac{i}{\omega_0} \frac{\partial}{\partial T} (|A|^2 A) \right), \quad (1)$$

where the amplitude of the pulse is represented by $A(z, T)$ which is a function of the transmission distance z and the delay time T defined by $T=t-z/v_g$. α is the transmission loss taken to be 7 dB/cm [27]. The nonlinear coefficient γ can be calculated by the

formula $\gamma = \omega_0 n_2 / c A_{\text{eff}}$, where the Kerr refractive index n_2 is $9.2 \times 10^{-19} \text{ m}^2/\text{W}$ [22]. $\beta^{(m)}$ stands for the higher-order dispersion coefficient term in the Taylor series expansion of the propagation constant β near the central frequency ω_0 .

The first-order coherence of the SC can be calculated by [28]

$$g_{12}^{(1)}(\lambda) = \frac{\langle A_1^*(\lambda) A_2(\lambda) \rangle}{\sqrt{\langle |A_1(\lambda)|^2 \rangle \langle |A_2(\lambda)|^2 \rangle}}, \quad (2)$$

where $A(\lambda)$ stands for the spectral amplitude of the SC with random input noise. The noise can be expressed by [29]

$$n = \eta \hat{N} \exp(i2\pi \hat{U}). \quad (3)$$

where the amplitude of the noise relative to the input pulse is represented by η , and \hat{N} and \hat{U} are the random variables that obey the standard normal distribution and uniform distribution, respectively.

3. Waveguide design and characteristics

A slot SiC waveguide is designed to achieve the relatively flattened dispersion with four ZDWs, which facilitates the exploration of rich nonlinear effects for the SC generation, as shown in Fig. 1(a). The waveguide consists of the SiC claddings and SiO₂ slot and substrate. W denotes the width, and H_u , H_l , and H_s represent for the heights of the upper cladding, the lower cladding, and the slot region, respectively. In this simulation, the wavelength-dependent refractive index of the SiC can be obtained by the Sellmeier equation [30]. The mode field distributions of the quasi-TM mode calculated at wavelengths 0.8, 1.6, 2.4, and 3.2 μm are shown in Fig. 1(b). It can be seen from Fig. 1(b) that most of the mode field energy is confined in the lower strip part at the shorter wavelength. As the wavelength increases, a quantity of energy

penetrates to the slot region.

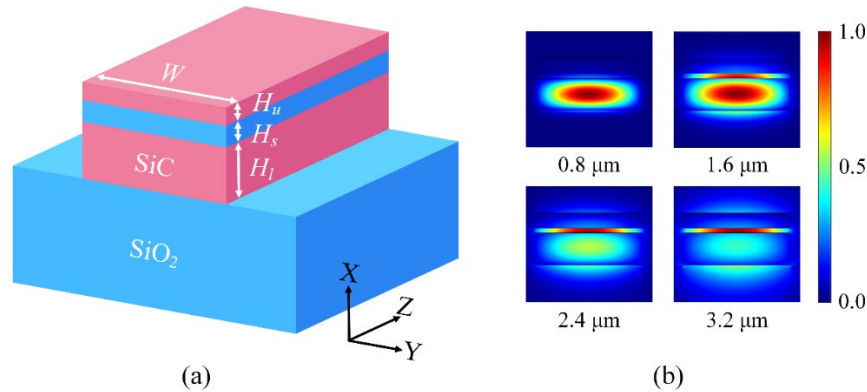


Fig. 1. (a) Sketch of the slot SiC waveguide. (b) Mode field distributions of the quasi-TM mode

calculated at wavelengths 0.8, 1.6, 2.4, and 3.2 μm , respectively.

The dispersion profiles can be tailored by adjusting the geometrical parameters of the waveguide, as shown in Figs. 2(a-d). Fig. 2(a) shows the dispersion curves of the waveguide with W varying from 1350 to 1950 nm. From Fig. 2(a), as W increases, the first peak of the dispersion curve drops obviously and the second peak rises slightly. As seen from Fig. 2(b), the increase of H_u has a similar effect to that of increasing W , except that the red-shift of the fourth ZDW is more significant. As shown in Fig. 2(c), the whole curve moves towards the normal dispersion regime by reducing H_l . Fig. 2(d) shows that with the decrease of H_s , the first peak of the dispersion curve decreases while the second peak increases. When the optimized geometrical parameters are chosen as $W = 1950$ nm, $H_u = 280$ nm, $H_l = 590$ nm, and $H_s = 85$ nm, a flat dispersion curve with the four ZDWs can be obtained. The calculated dispersion coefficient D and nonlinear coefficient γ of the waveguide are shown in Fig. 3. From Fig. 3, the four ZDWs are approximately located at 1089, 1656, 2222, and 3113 nm, respectively. In addition, γ decreases monotonically as the wavelength increases. And at the pump

wavelengths of 1300 and 2450 nm, γ is about 5.52 and 0.76 /m/W, respectively.

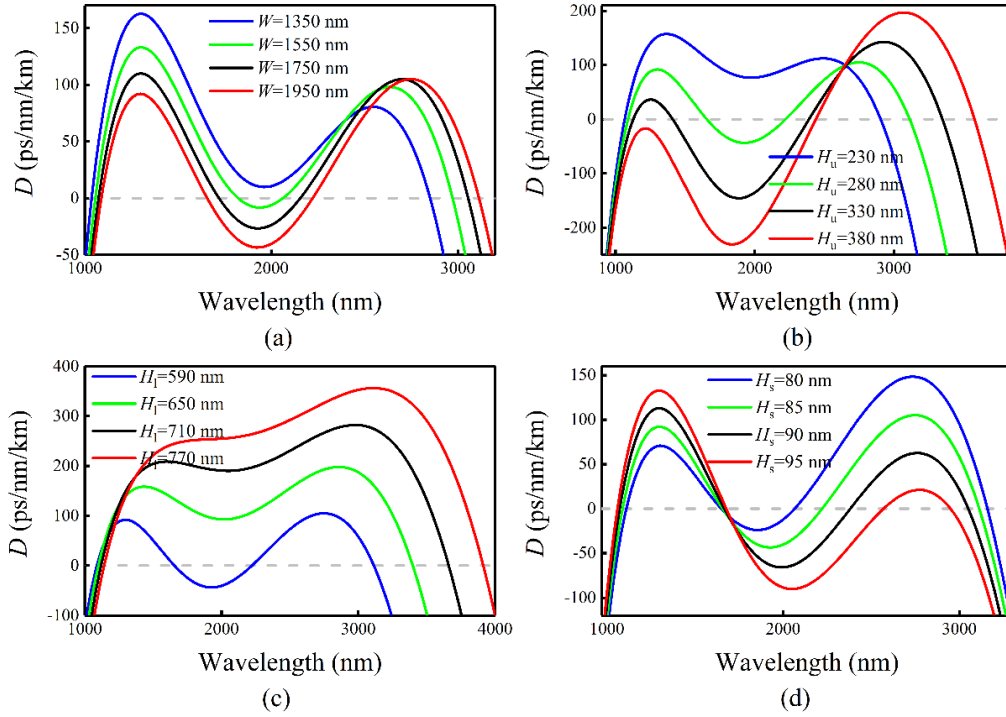


Fig. 2. Variations in the dispersion curves of the proposed waveguide with different

(a) W , (b) H_u , (c) H_l , and (d) H_s , respectively.

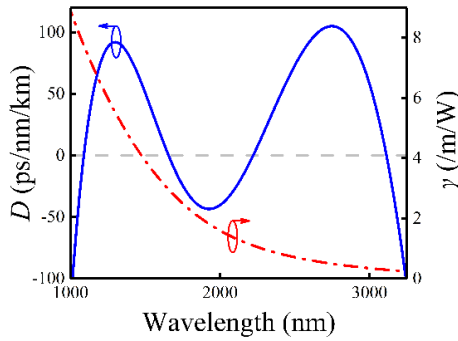


Fig. 3. The calculated dispersion coefficient D and nonlinear coefficient γ as functions of wavelength

when $W = 1950$ nm, $H_u = 280$ nm, $H_l = 590$ nm, and $H_s = 85$ nm are chosen.

4. Simulation results and discussion

Utilizing the Runge-Kutta method to solve Eq. (1), the SC generation inside the designed slot SiC waveguide can be numerically studied. The proposed waveguide

will be pumped near the first and third ZDW, respectively, and the effects of the pump wavelength, peak power, pulse width, and waveguide length on the SC generation will be investigated.

4.1. Pumping near the first ZDW

The input pulse is a chirp-free hyperbolic secant pulse with peak power of 200 W and width of 100 fs. When the pump wavelength is changed from 1220 to 1380 nm, the temporal and spectral profiles and the first-order coherence of the SC at the output end of the 5.4-mm-long SiC waveguide are shown in Figs. 4(a-c). From Fig. 4(a), the temporal pulse becomes narrower with the increase of the pump wavelength, and the split peaks appear. From Fig. 4(b), with the increase of the pump wavelength, the increasing β_2 leads to the enhancement of the dispersion effect. The higher-order soliton is formed under the combined influence of the dispersion effect and self-phase modulation (SPM) effect because the pump pulse works in the anomalous dispersion region of the waveguide. Under the action of the higher-order dispersion, the higher-order soliton will split into the fundamental solitons. At the same time, when the resonance matching condition is satisfied, the blue-shifted dispersion waves will be observed at the shorter wavelength side. The existence of the second ZDW inhibits the red-shift of the soliton. Fortunately, the FWM effect further extends the spectral width due to the presence of the third ZDW. When the pump wavelength continues to increase above 1300 nm, no significant spectral broadening is observed. This is because the maximum value of β_2 appears at wavelength 1300 nm, where the dispersion effect is strong. Besides, as the pump wavelength increases, the flatness of

the generated SC decreases, but the coherence of the SC is close to 1, as shown in Fig. 4(c).

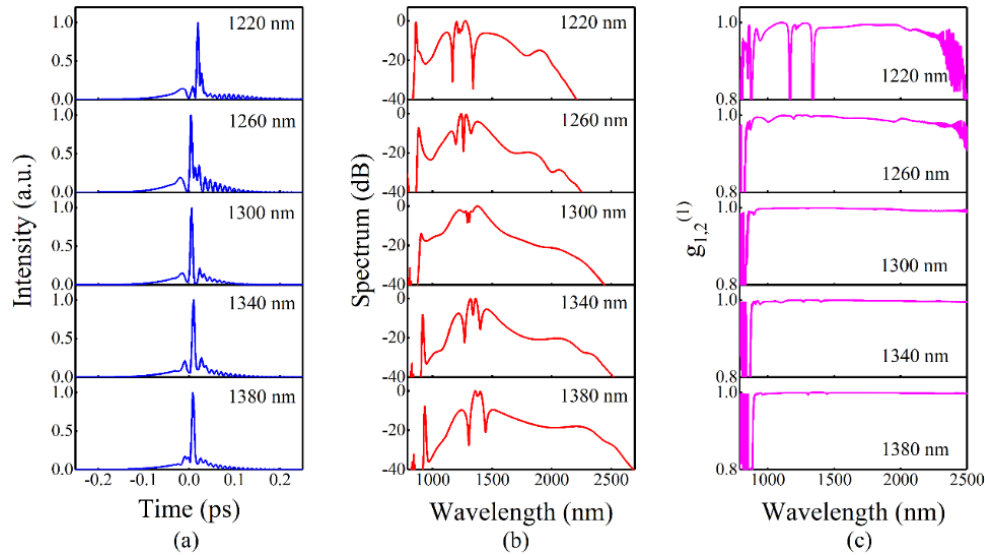


Fig. 4. (a) Temporal and (b) spectral profiles and (c) the first-order coherence

of the generated SC for different pump wavelengths.

When the 5.4-mm-long SiC waveguide is pumped by the pulse with wavelength of 1300 nm and width of 100 fs, the temporal and spectral profiles and the coherence of the SC generated with different peak powers are shown in Figs. 5(a-c). As shown in Fig. 5(a), when the peak power increases from 150 to 200 W, the pulse at the output end of the waveguide is greatly compressed. As seen from Fig. 5(b), with the increase of the peak power, the intensity of the SPM effect increases, and the order of the soliton also increases, thus splitting into more fundamental solitons. The enhancement of some nonlinear effects gradually widens the optical spectrum. However, when the peak power continues to increase above 200 W, the spectral width does not increase obviously, and the modulation instability leads to the decrease of the flatness. Moreover, the coherence of the SC generated at the output end of the waveguide also

deteriorates, as shown in Fig. 5(c).

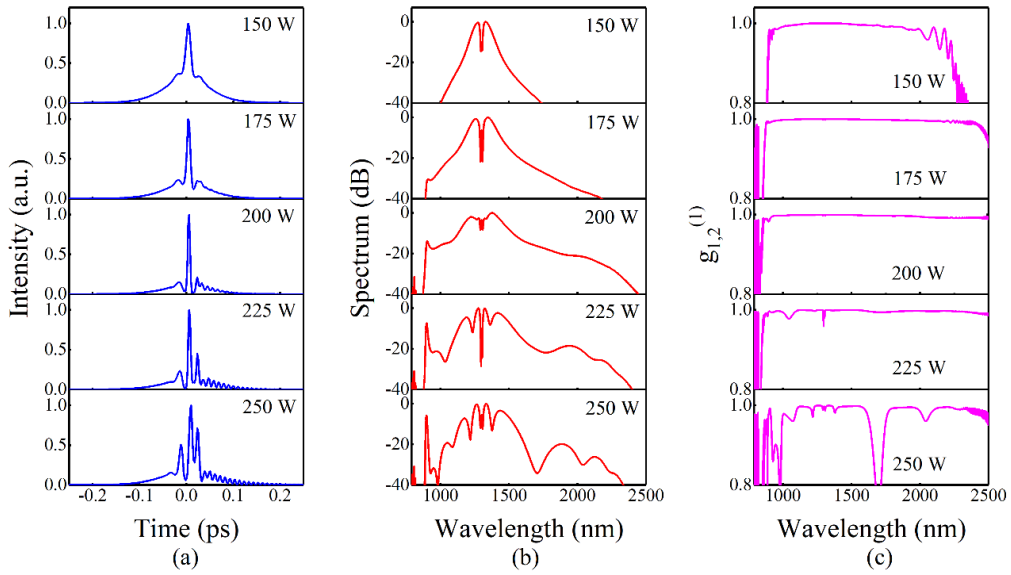


Fig. 5. (a) Temporal and (b) spectral profiles and (c) the first-order coherence

of the generated SC for different pump peak powers.

When the pump wavelength, peak power, and waveguide length are set to 1300 nm, 200 W, and 5.4 mm, respectively, the effect of the pulse width on the SC generation is shown in Figs. 6(a-c). From Fig. 6(a), when the pulse width changes from 90 to 100 fs, the output pulse width decreases slightly. As the pulse width continues to increase, the output pulse width becomes larger. As shown in Fig. 6(b), when the pulse width is increased to 100 fs, the spectral width is larger, and the flatness is also improved. This main reason is considered that for the larger pulse width, the higher order of the soliton is generated. When the multiple fundamental solitons generated by the splitting of the higher-order soliton approach the ZDW, the third-order dispersion will have a great impact, thus widening the spectrum at the longer wavelength side. However, for the larger pulse width, the pulse energy will be greatly dispersed, which is not conducive to the spectral broadening. This is also why

the spectral width decreases when the pulse width continues to increase above 100 fs.

As shown in Fig. 6(c), as the pulse width decreases, the coherence of the SC becomes better, approaching 1.

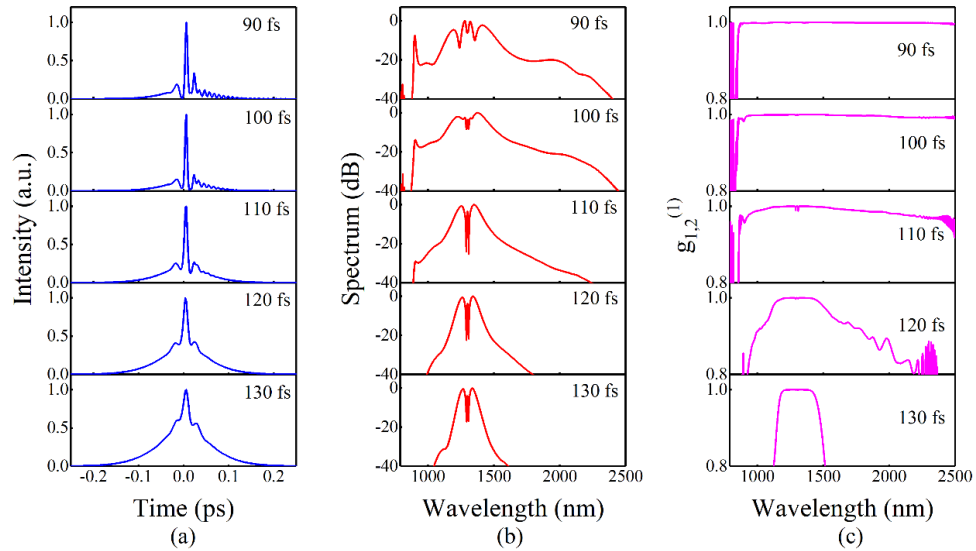


Fig. 6. (a) Temporal and (b) spectral profiles and (c) the first-order coherence

of the generated SC for different pulse widths.

Figs. 7(a-c) show the effect of the waveguide length on the SC generation when the pump pulse with wavelength of 1300 nm, peak power of 200 W, and width of 100 fs is used. It can be observed from Figs. 7(a) and 7(b) that with the increase of the waveguide length, the output pulse is gradually compressed, and the optical spectrum is broadened more obviously. This is because the optical spectrum is initially broadened under the action of the SPM effect, and further broadened by the soliton fission and cross-phase modulation as the waveguide length increases. At a waveguide length of about 5.1 mm, there is a distinct peak at the shorter wavelength side, which means that a dispersion wave appears in the normal dispersion region. The shape and spectral width of the SC do not change significantly when the waveguide length

increases above 5.4 mm. As shown in Fig. 7(c), for the waveguide length of 4.5-5.7 mm, the coherence curves of the SC are relatively flat and approximately equal to 1.

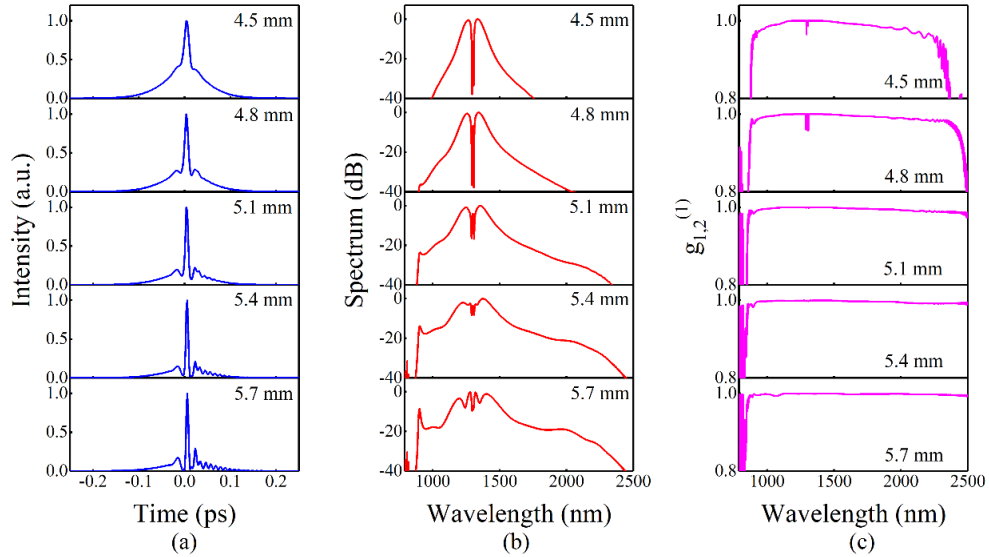


Fig. 7. (a) Temporal and (b) spectral profiles and (c) the first-order coherence

of the generated SC for different waveguide lengths.

Figs. 8(a) and 8(b) show the evolutions of the temporal and spectral profiles as the pump pulse propagates in the designed SiC waveguide. As shown in Fig. 8(a), as the propagation distance increases, the pulse is gradually compressed due to the combined dispersion and nonlinear effects. As shown in Fig. 8(b), at the initial stage of the pulse propagation, the optical spectrum is symmetrically extended by the SPM effect. As the propagation distance continues to increase, the nonlinear effects including soliton fission, dispersion wave, and cross-phase modulation can further broaden the optical spectrum asymmetrically. Finally, a near-infrared SC covering from 873 to 2444 nm is obtained in a 5.4-mm-long SiC waveguide at the -40 dB level, spanning 1.49 octaves.

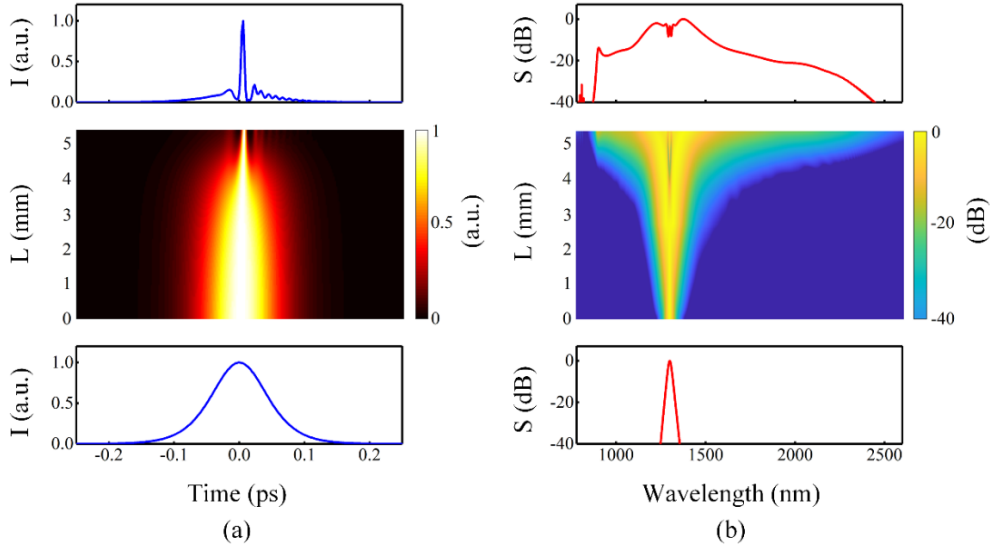


Fig. 8. Evolutions of (a) temporal pulse and (b) optical spectrum when the pump pulse with wavelength of 1300 nm, width of 100 fs, and peak power of 200 W is used. The bottom and top of (a) are the input and output pulses. The bottom and top of (b) are the corresponding input and output optical spectra.

The intensity, optical spectrum, and length are expressed as ‘ T ’, ‘ S ’, and ‘ L ’, respectively.

4.2. Pumping near the third ZDW

In the following, we will focus on the SC generation pumped near the third ZDW. Figs. 9(a-c) show the temporal and spectral profiles and the first-order coherence of the generated SC at the output end of the 2.2-mm-long SiC waveguide when the wavelength of the pump pulse with peak power of 2.6 kW and width of 100 fs is changed from 2450 to 2530 nm. As shown in Fig. 9(a), as the pump wavelength increases, there is no evident change in the temporal pulse. As shown in Fig. 9(b), with the increase of the pump wavelength, the spectral width doesn’t change significantly, but the whole spectrum is slightly red-shifted, and the flatness of the SC is decreased. Fig. 9(c) shows the coherence of the generated SCs. From Fig. 9(c), the obtained mid-infrared SCs have good coherence.

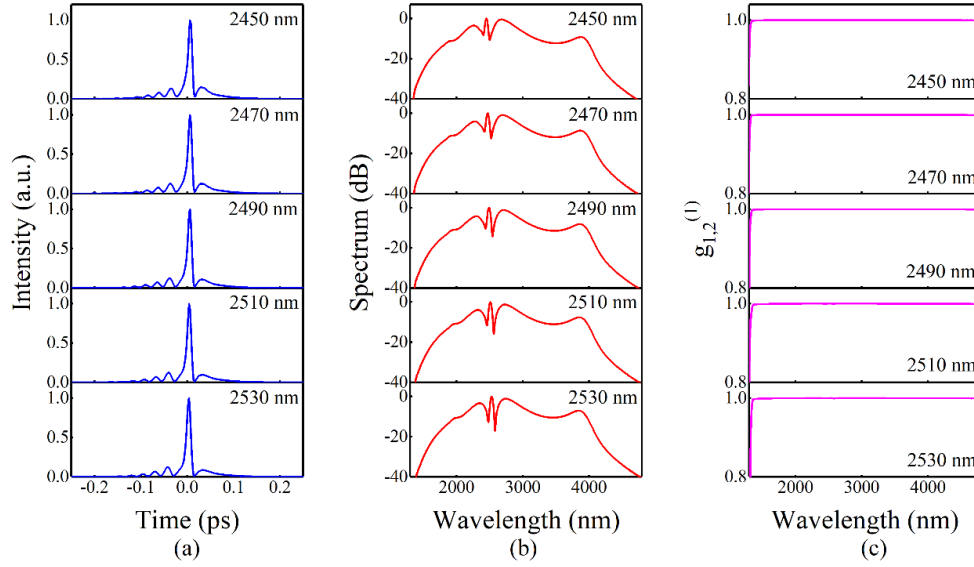


Fig. 9. (a) Temporal and (b) spectral profiles and (c) the first-order coherence

of the generated SC for different pump wavelengths.

When the peak power of the pump pulse with wavelength of 2450 nm and width of 100 fs is chosen as 1.0, 1.4, 1.8, 2.2, and 2.6 kW, respectively, the temporal and spectral profiles and the first-order coherence of the SC generated at the output end of the 2.2-mm-long SiC waveguide are shown in Figs. 10(a-c). From Fig. 10(a), with the increase of the peak power, the compression degree of the output pulse gradually increases. When the peak power increases from 1.0 to 2.6 kW, the spectral width of the output pulse increases gradually, as shown in Fig. 10(b). This is because the order of the soliton increases with the increase of the peak power, and the optical spectrum of the pulse is obviously widened. From Fig. 10(c), the generated SC remains good coherence over the spectral range of -40 dB bandwidth. When the peak power continues to increase above 2.6 kW, the amplitude of the spectral broadening decreases.

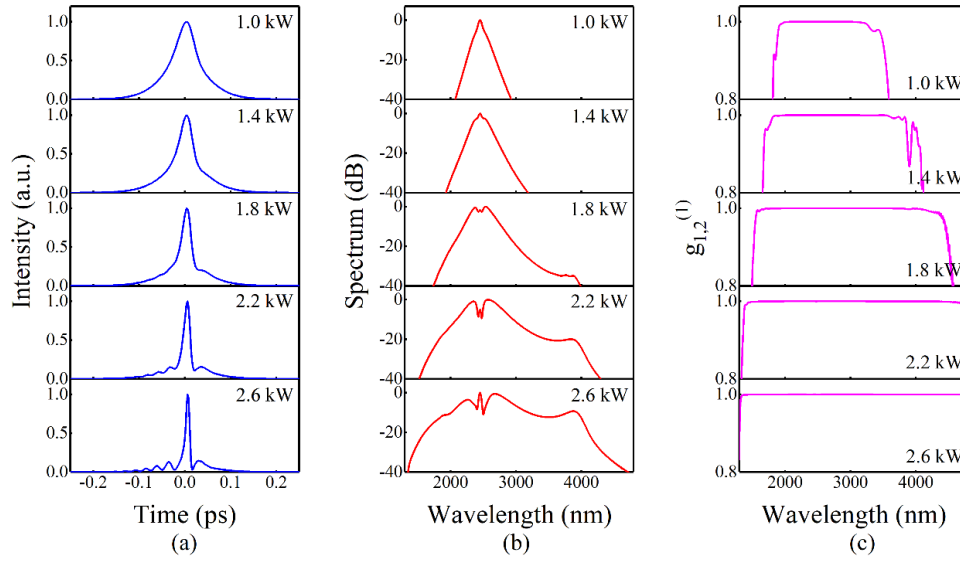


Fig. 10. (a) Temporal and (b) spectral profiles and (c) the first-order coherence

of the generated SC for different pump peak powers.

The wavelength and peak power of the pump pulse is set to 2450 nm and 2.6 kW, respectively. When the width of the pump pulse changes from 90, to 100, to 110, to 120, and to 130 fs, respectively, the temporal and spectral profiles and the coherence of the SC obtained at the output end of the 2.2-mm-long SiC waveguide are shown in Figs. 11(a-c). As shown in Fig. 11(a), with the increase of the pulse width, the compression degree of the output pulse decreases. From Fig. 11(b), the increase of the pulse width makes the pulse energy gradually dispersed, and it will lead to the increase of the soliton fission length, which may result in the insufficient propagation distance to completely split the soliton and is not conducive to the spectral broadening. In addition, the flatness of the SC generated for the pulse width of 100 fs is better than that for the pulse width of 90 fs. Therefore, the pulse width is set to 100 fs. At this time, the coherence of the generated SC is close to 1, as seen from Fig. 11(c).

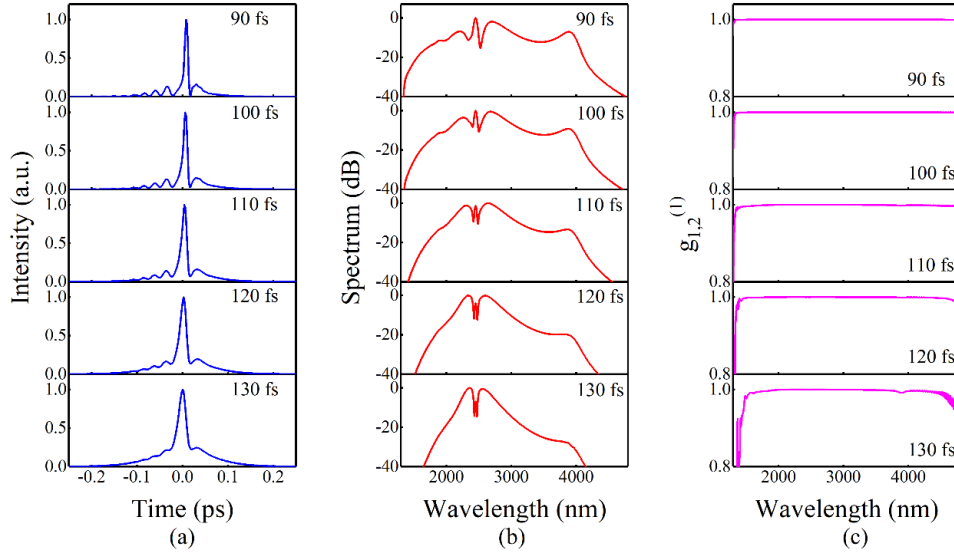


Fig. 11. (a) Temporal and (b) spectral profiles and (c) the first-order coherence

of the generated SC for different pulse widths.

When the pump pulse with wavelength of 2450 nm, peak power of 2.6 kW, and width of 100 fs is launched into the SiC waveguides with different lengths, the temporal and spectral profiles and the coherence of the generated SC are shown in Figs. 12(a-c). As shown in Fig. 12(a), the width of the output pulse gradually decreases with the increase of the waveguide length. From Fig. 12(b), when the waveguide length is less than 2.2 mm, the optical spectrum is broadened mainly by the SPM effect. However, when the waveguide length is larger than 2.2 mm, the higher-order dispersion leads to the increase of the side-lobe pulse energy, and the peak of the pulse moves to the trailing edge under the combined action of the higher-order dispersion and self-steepening effects, which both disperse the pulse energy. Besides, the continuous growth of the waveguide length will bring much higher loss, which will suppress the further spectral broadening. From Fig. 12(c), the coherence is better when the waveguide length is chosen as 2.2 mm.

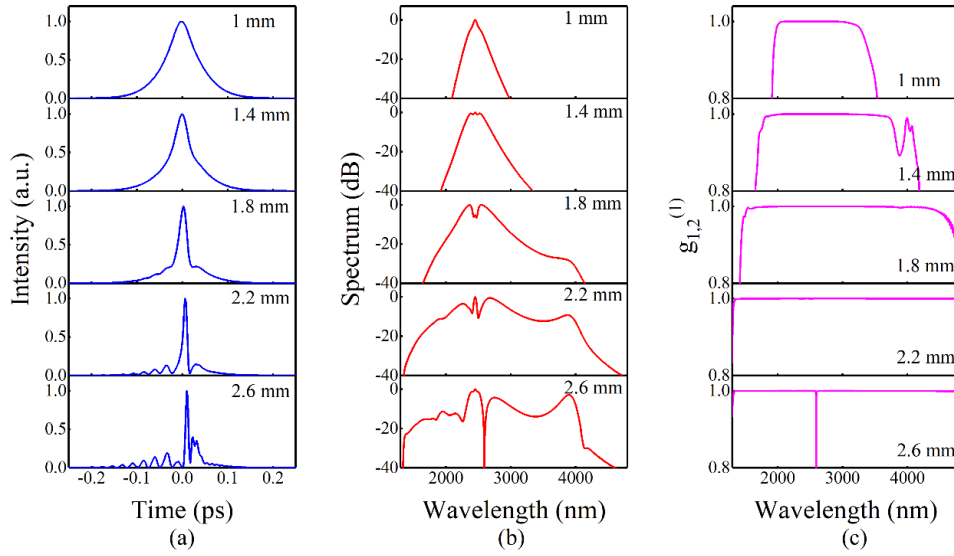


Fig. 12. (a) Temporal and (b) spectral profiles and (c) the first-order coherence

of the generated SC for different waveguide lengths.

When a hyperbolic secant pulse with wavelength of 2450 nm, width of 100 fs, and peak power of 2.6 kW is propagated inside the designed SiC waveguide, the corresponding evolutions of the temporal and spectral profiles with the propagation distance are shown in Figs. 13(a) and 13(b). As shown in Fig. 13(a), the pulse width gradually decreases with the increase of the propagation distance. It can be seen from Fig. 13(b) that at the initial stage, the symmetric broadening of the optical spectrum is caused by the SPM effect. Subsequently, various nonlinear effects allow the optical spectrum to be asymmetrically extended toward the longer and shorter wavelength sides. Finally, a mid-infrared SC covering from 1349 to 4727 nm is generated at the output end of the 2.2-mm-long SiC waveguide, covering about 1.81 octaves.

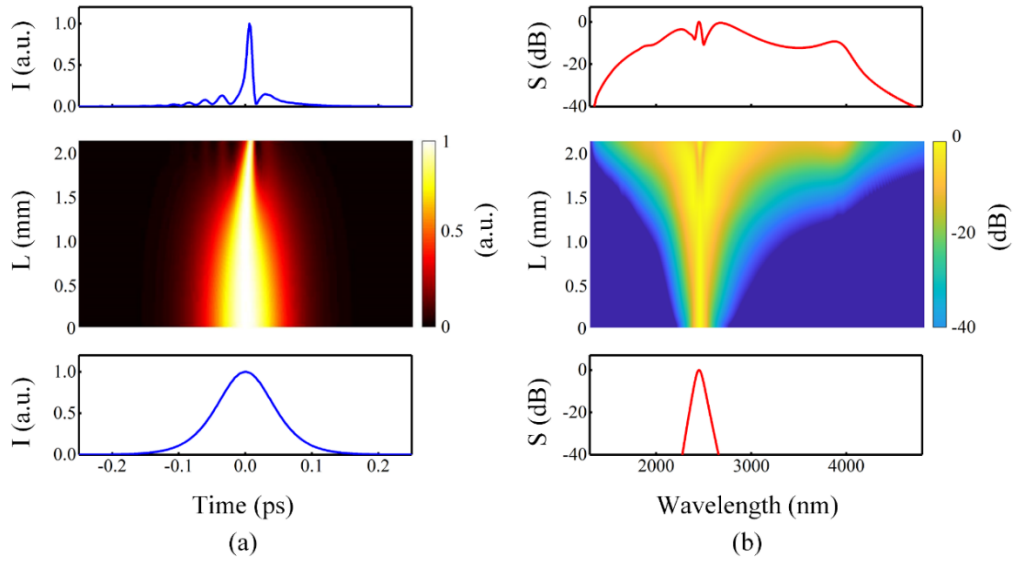


Fig. 13. Evolutions of (a) temporal pulse and (b) optical spectrum when the pump pulse with wavelength of 2450 nm, width of 100 fs, and peak power of 2.6 kW is used. The bottom and top of (a) are the input and output pulses. The bottom and top of (b) are the corresponding input and output optical spectra. The intensity, optical spectrum, and length are expressed as ‘ I ’, ‘ S ’, and ‘ L ’, respectively.

Based on the broadband SCs with good coherence, we could acquire optical frequency combs, which have attracted wide attention due to their potential in high precision spectroscopy, communication, optical atomic clock, and metrology [31-36]. In this work, a pulse train including 50 pulses with wavelength of 1300 nm, peak power of 200 W, width of 100 fs, and repetition rate of 1 GHz is taken as the pump source. After the propagation in the 5.4-mm-long slot SiC waveguide, the SC-based frequency comb is shown in Fig. 14(a). Figs. 14(b) and 14(c) are the zoom-in views of the frequency comb obtained at 198 THz/1515.15 nm and 245 THz/1224.49 nm with a sampling bandwidth of 5 GHz, for the convenience of observing the comb structure. It can be said that a near-infrared frequency comb spanning from 122.75 THz/2444

nm to 343.64 THz/873 nm with equal interval and stable amplitude is attained on the basis of generating octave and highly coherent near-infrared SC from the proposed slot SiC waveguide. Similarly, when the wavelength, peak power, and width of the pulse train are set to 2450 nm, 2.6 kW, and 100 fs, respectively, the generated mid-infrared frequency comb is shown in Fig. 15. Figs. 15(b) and 15(c) are the zoom-in views of the frequency comb obtained at 90 THz/3333.33 nm and 132 THz/2272.73 nm with a sampling bandwidth of 5 GHz.

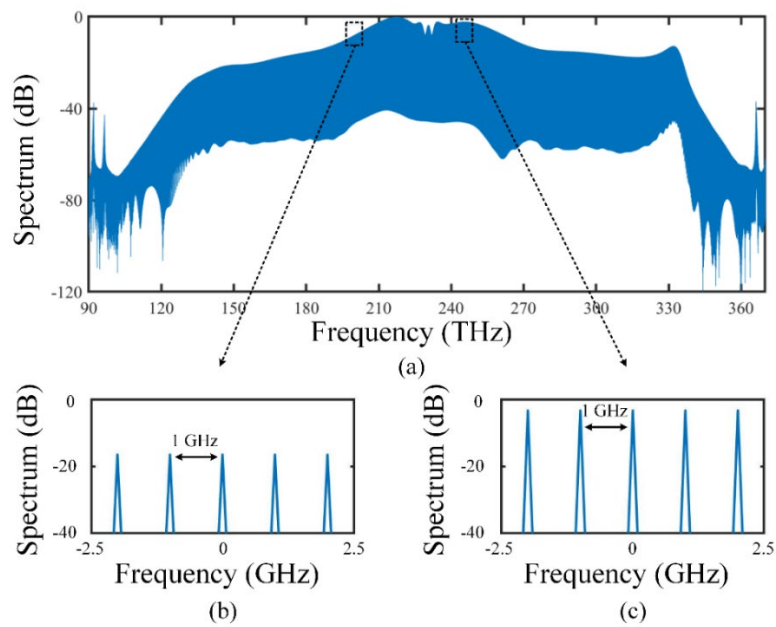


Fig. 14. (a) The SC-based frequency comb generated when the wavelength of the pulse train

is 1300 nm. The zoom-in views of the frequency comb at

(b) 198 THz/1515.15 nm and (c) 245 THz/1224.49 nm.

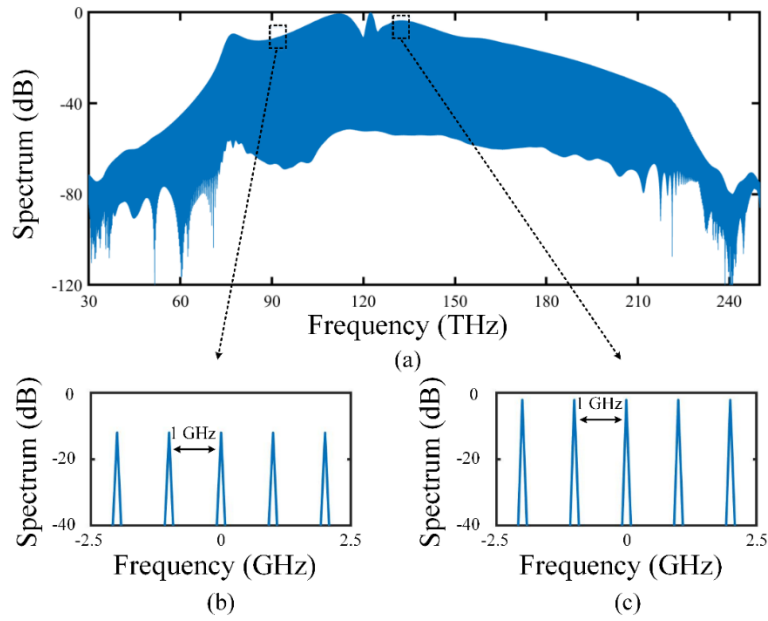


Fig. 15. (a) The SC-based frequency comb generated when the wavelength of the pulse train is 2450 nm. The zoom-in views of the frequency comb at (b) 90 THz/3333.33 nm and (c) 132 THz/2272.73 nm.

5. Conclusion

In summary, a slot SiC waveguide with four ZDWs is proposed for the SC and frequency comb generations. The effects of the pump wavelength, peak power, pulse width, and waveguide length on the SC generation are investigated. When the pump wavelength, peak power, pulse width, and waveguide length are chosen as 1300 nm, 200 W, 100 fs, and 5.4 mm, respectively, the generated near-infrared SC covers from 873 to 2444 nm at -40 dB level, spanning 1.49 octaves. In contrast, when the pump wavelength, peak power, pulse width, and waveguide length are chosen as 2450 nm, 2.6 kW, 100 fs, and 2.2 mm, the generated mid-infrared SC extends from 1349 to 4727 nm, covering 1.81 octaves. Besides, by using the pump pulse train containing 50 pulses at a repetition rate of 1 GHz, the near-infrared and mid-infrared SC-based

frequency combs are obtained. The results of this paper provide a feasible scheme for the SC and frequency comb generations, and will promote the further researches on the SC and frequency comb sources.

Acknowledgements

This work was supported by the National Natural Science Foundation of China (Grant No. 61875238).

References

- [1] Z. Kang, C. Mei, L. Zhang, Z. Zhang, J. Evans, Y. Cheng, K. Zhu, X. Zhang, D. Huang, Y. Li, J. He, Q. Wu, B. Yan, K. Wang, X. Zhou, K. Long, F. Li, Q. Li, S. Wang, J. Yuan, P. K. A. Wai, S. He, Advanced progress on $\chi^{(3)}$ nonlinearity in chip-scale photonic platforms (Invited Review), Prog. Electromagn. Res. 170 (2021) 17-62, <https://doi.org/10.2528/PIER20122108>.
- [2] A. G. N. Chaitanya, T. S. Saini, A. Kumar, R. K. Sinha, Ultra broadband mid-IR supercontinuum generation in $\text{Ge}_{11.5}\text{As}_{24}\text{Se}_{64.5}$ based chalcogenide graded-index photonic crystal fiber: design and analysis, Appl. Optics 55 (36) (2016) 10138-10145, <https://doi.org/10.1364/AO.55.010138>.
- [3] H. Ou, S. Dai, P. Zhang, Z. Liu, X. Wang, F. Chen, H. Xu, B. Luo, Y. Huang, R. Wang, Ultrabroad supercontinuum generated from a highly nonlinear Ge–Sb–Se fiber, Opt. Lett. 41 (14) (2016) 3201-3204, <https://doi.org/10.1364/OL.41.003201>.
- [4] L. Carletti, M. Sinobad, P. Ma, Y. Yu, D. Allieux, R. Orobtcouk, M. Brun, S. Ortiz, P. Labeye, J. M. Hartmann, S. Nicoletti, S. Madden, B. Luther-Davies, D. J. Moss, C. Monat, C. Grillet, Mid-infrared nonlinear optical response of Si-Ge waveguides with ultra-short optical pulses, Opt. Express 23 (25)

(2015) 32202-32214, <https://doi.org/10.1364/OE.23.032202>.

[5] J. Hu, J. Meyer, K. Richardson, L. Shah, Feature issue introduction: mid-IR photonic materials, *Opt. Mater. Express* 3 (9) (2013) 1571-1575, <https://doi.org/10.1364/OME.3.001571>.

[6] L. Zhang, A. M. Agarwal, L. C. Kimerling, J. Michel, Nonlinear Group IV photonics based on silicon and germanium: from near-infrared to mid-infrared, *Nanophotonics* 3 (4-5) (2014) 247-268, <https://doi.org/10.1515/nanoph-2013-0020>.

[7] Y. Yu, X. Gai, T. Wang, P. Ma, R. Wang, Z. Yang, D. Y. Choi, S. Madden, B. Luther-Davies, Mid-infrared supercontinuum generation in chalcogenides, *Opt. Mater. Express* 3 (8) (2013) 1075-1086, <https://doi.org/10.1364/OME.3.001075>.

[8] H. Saghaei, V. Van, Broadband mid-infrared supercontinuum generation in dispersion-engineered silicon-on-insulator waveguide, *J. Opt. Soc. Am. B* 36 (2) (2019) A193-A202, <https://doi.org/10.1364/JOSAB.36.00A193>.

[9] J. Yuan, Z. Kang, F. Li, X. Zhang, X. Sang, Q. Wu, B. Yan, K. Wang, X. Zhou, K. Zhong, G. Zhou, C. Yu, C. Lu, H. Y. Tam, P. K. A. Wai, Mid-infrared octave-spanning supercontinuum and frequency comb generation in a suspended germanium-membrane ridge waveguide, *J. Lightwave Technol.* 35 (14) (2017) 2994-3002, <https://doi.org/10.1109/JLT.2017.2703644>.

[10] M. Sinobad, A. DellaTorre, R. Armand, B. Luther-Davies, P. Ma, S. Madden, A. Mitchell, D. J. Moss, J. M. Hartmann, J. M. Fedeli, C. Monat, C. Grillet, Mid-infrared supercontinuum generation in silicon-germanium all-normal dispersion waveguides, *Opt. Lett.* 45 (18) (2020) 5008-5011, <https://doi.org/10.1364/OL.402159>.

[11] C. Lafforgue, S. Guerber, J. M. Ramirez, G. Marcaud, C. Alonso-Ramos, X. L. Roux, D. Marris-Morini, E. Cassan, C. Baudot, F. Boeuf, S. Cremer, S. Monfray, L. Vivien, Broadband

supercontinuum generation in nitrogen-rich silicon nitride waveguides using a 300 mm industrial platform, *Photonics Res.* 8 (3) (2020) 352-358, <https://doi.org/10.1364/PRJ.379555>.

[12] S. Jing, C. Mei, K. Wang, J. Yuan, B. Yan, X. Sang, C. Yu, Broadband and highly coherent supercontinuum generation in a suspended As_2S_3 , ridge waveguide, *Opt. Commun.* 428 (2018) 227-232, <https://doi.org/10.1016/j.optcom.2018.07.071>.

[13] T. S. Saini, U. K. Tiwari, R. K. Sinha, Design and analysis of dispersion engineered rib waveguides for on-chip mid-infrared supercontinuum, *J. Lightwave Technol.* 36 (10) (2018) 1993-1999, <https://doi.org/10.1109/JLT.2018.2800282>.

[14] J. É. Tremblay, M. Malinowski, K. A. Richardson, S. Fathpour, M. C. Wu, Picojoule-level octave-spanning supercontinuum generation in chalcogenide waveguides, *Opt. Express* 26 (16) (2018) 21358-21363, <https://doi.org/10.1364/OE.26.021358>.

[15] J. Lu, X. Liu, A. W. Bruch, L. Zhang, J. Wang, J. Yan, H. X. Tang, Ultraviolet to mid-infrared supercontinuum generation in single-crystalline aluminum nitride waveguides, *Opt. Lett.* 45 (16) (2020) 4499-4502, <https://doi.org/10.1364/OL.398257>.

[16] Y. Cheng, J. Lai, J. Yuan, C. Mei, X. Zhou, Q. Wu, B. Liu, B. Yan, K. Wang, C. Yu, X. Sang, Highly coherent and multi-octave mid-infrared supercontinuum generations in a reverse-strip AlGaAs waveguide with three zero-dispersion wavelengths, *Appl. Optics* 60 (31) (2021) 9994-10001, <https://doi.org/10.1364/AO.440682>.

[17] U. D. Dave, C. Ciret, S. P. Gorza, S. Combrie, A. D. Rossi, F. Raineri, G. Roelkens, B. Kuyken, Dispersive-wave-based octave-spanning supercontinuum generation in InGaP membrane waveguides on a silicon substrate, *Opt. Lett.* 40 (15) (2015) 3584-3587, <https://doi.org/10.1364/OL.40.003584>.

[18] Y. Zheng, M. Pu, A. Yi, B. Chang, T. You, K. Huang, A. N. Kamel, M. R. Henriksen, A. A.

Jørgensen, X. Ou, H. Ou, High-quality factor, high-confinement microring resonators in 4H-silicon carbide-on-insulator, *Opt. Express* 27 (9) (2019) 13053-13060, <https://doi.org/10.1364/OE.27.013053>.

[19] A. Yi, Y. Zheng, H. Huang, J. Lin, Y. Yan, T. You, K. Huang, S. Zhang, C. Shen, M. Zhou, W. Huang, J. Zhang, S. Zhou, H. Ou, X. Ou, Wafer-scale 4H-silicon carbide-on-insulator (4H-SiCOI) platform for nonlinear integrated optical devices, *Opt. Mater.* 107 (2020) 109990, <https://doi.org/10.1016/j.optmat.2020.109990>.

[20] C. Wang, Z. Fang, A. Yi, B. Yang, Z. Wang, L. Zhou, C. Shen, Y. Zhu, Y. Zhou, R. Bao, Z. Li, Y. Chen, K. Huang, J. Zhang, Y. Cheng, X. Ou, High-Q microresonators on 4H-silicon-carbide-on-insulator platform for nonlinear photonics, *Light: Science & Applications* 10 (1) (2021) 1-11, <https://doi.org/10.1038/s41377-021-00584-9>.

[21] S. Wang, M. Zhan, G. Wang, H. Xuan, W. Zhang, C. Liu, C. Xu, Y. Liu, Z. Wei, X. Chen, 4H-SiC: a new nonlinear material for midinfrared lasers, *Laser Photonics Rev.* 7 (5) (2013) 831-838, <https://doi.org/10.1002/lpor.201300068>.

[22] Y. Zheng, M. Pu, A. Yi, X. Ou, H. Ou, 4H-SiC microring resonators for nonlinear integrated photonics, *Opt. Lett.* 44 (23) (2019) 5784-5787, <https://doi.org/10.1364/OL.44.005784>.

[23] P. Xing, D. Ma, L. C. Kimerling, A. M. Agarwal, D. T. H. Tan, High efficiency four wave mixing and optical bistability in amorphous silicon carbide ring resonators, *APL Photonics* 5 (7) (2020) 076110, <https://doi.org/10.1063/5.0009692>.

[24] G. Xu, J. Yan, Z. Chen, T. Huang, Z. Cheng, P. P. Shum, G. Brambilla, Design of germanium-silicon carbide hybrid waveguides for mid-infrared third-order parametric conversion, *Opt. Commun.* 456 (2020) 124668, <https://doi.org/10.1016/j.optcom.2019.124668>.

[25] Y. Zheng, M. Pu, P. Guan, A. Yi, L. K. Oxenløwe, X. Ou, H. Ou, Supercontinuum Generation in

Dispersion Engineered 4H-SiC-on-Insulator Waveguides at Telecom Wavelengths, 2020 Conference on Lasers and Electro-Optics (CLEO) (2020) 1-2, https://doi.org/10.1364/CLEO_SI.2020.SM4R.7.

[26] J. M. Dudley, G. Genty, S. Coen, Supercontinuum generation in photonic crystal fiber, *Rev. Mod. Phys.* 78 (4) (2006) 1135, <https://doi.org/10.1103/RevModPhys.78.1135>.

[27] J. Cardenas, M. Yu, Y. Okawachi, C. B. Poitras, R. K. W. Lau, A. Dutt, A. L. Gaeta, M. Lipson, Optical nonlinearities in high-confinement silicon carbide waveguides, *Opt. Lett.* 40 (17) (2015) 4138-4141, <https://doi.org/10.1364/OL.40.004138>.

[28] F. Li, Q. Li, J. Yuan, P. K. A. Wai, Highly coherent supercontinuum generation with picosecond pulses by using self-similar compression, *Opt. Express* 22 (22) (2014) 27339-27354, <https://doi.org/10.1364/OE.22.027339>.

[29] J. Lai, J. Yuan, Y. Cheng, C. Mei, X. Zhou, Q. Wu, B. Yan, K. Wang, K. Long, C. Yu, X. Sang, Dispersion-engineered T-type germanium waveguide for mid-infrared supercontinuum and frequency comb generations in all-normal dispersion region, *OSA Continuum* 3 (9) (2020) 2320-2331, <https://doi.org/10.1364/OSAC.399941>.

[30] M. Naftaly, J. F. Molloy, B. Magnusson, Y. M. Andreev, G. V. Lanskii, Silicon carbide—a high-transparency nonlinear material for THz applications, *Opt. Express* 24 (3) (2016) 2590-2595, <https://doi.org/10.1364/OE.24.002590>.

[31] A. Schliesser, N. Picqué, T. W. Hänsch, Mid-infrared frequency combs, *Nat. Photonics* 6 (2012) 440-449, <https://doi.org/10.1038/nphoton.2012.142>.

[32] T. W. Hänsch, N. Picqué, Laser spectroscopy and frequency combs, *Journal of Physics: Conference Series* 467 (2013) 012001, <https://doi.org/10.1088/1742-6596/467/1/012001>.

[33] T. Udem, R. Holzwarth, T. W. Hänsch, Optical frequency metrology, *Nature* 416 (2002) 233-237,

<https://doi.org/10.1038/416233a>.

[34] L. Chang, S. Liu, J. E. Bowers, Integrated optical frequency comb technologies, *Nat. Photonics* 16 (2022) 95-108, <https://doi.org/10.1038/s41566-021-00945-1>.

[35] J. Ye, H. Schnatz, L.W. Hollberg, Optical frequency combs: from frequency metrology to optical phase control, *IEEE J. Sel. Top. Quant.* 9 (4) (2003) 1041-1058, <https://doi.org/10.1109/JSTQE.2003.819109>.

[36] F. Li, J. Yuan, Z. Kang, Q. Li, P. K. A. Wai, Modeling frequency comb sources, *Nanophotonics* 5 (2) (2016) 292-315, <https://doi.org/10.1515/nanoph-2016-0030>.